ESI

Multifunctional Applications of a Dysprosium-Based Metal-Organic Chain with Single-Ion Magnet Behaviour

Belén Fernández,[a] Itziar Oyarzabal,[b] Eva Fischer-Fodor,[c,d] Sergiu Macavei,[e] Ignacio Sánchez,[a] José M. Seco,[b] Santiago Gómez-Ruiz [f,*] and Antonio Rodríguez-Diéguez[a,*]

Index:

1. Luminescence Properties

Experimental.
A Varian Cary-Eclipse fluorescence spectrofluorometer was used to obtain the fluorescence spectra. The spectrofluorometer was equipped with a xenon discharge lamp (peak power equivalent to 75 kW), Czerny–Turner monochromators, and a R-928 photomultiplier tube which is red sensitive (even 900 nm) with manual or automatic voltage controlled using Cary Eclipse software for Windows 95/98/NT system. The photomultiplier detector voltage was 700 V and the instrument excitation and emission slits were set at 5 and 5 nm, respectively.

Results.
For the photo-excitation of 320 nm, the most intense band was found at 380 nm, which is stronger than the two characteristic emission $^4F_{9/2} \rightarrow {}^6H_J$ transitions of Dy^{3+} ions. This strong emission is probably assigned to the π-π* charge-transfer interaction of the derivative pyridinic ligand. The existence of the ligand-based emission in the luminescence spectra of **1** suggests that the energy transfer from the ligand to the Dy center is less effective, and the pyridinic ligand is not perfect for the Dy^{3+} ion. However, the existence of the two characteristic emission bands of Dy^{3+} ions suggests that the "antenna effect" still exists between the triplet state of pyridinic ligand to the resonant emissive energy level of Dy^{3+} ion.

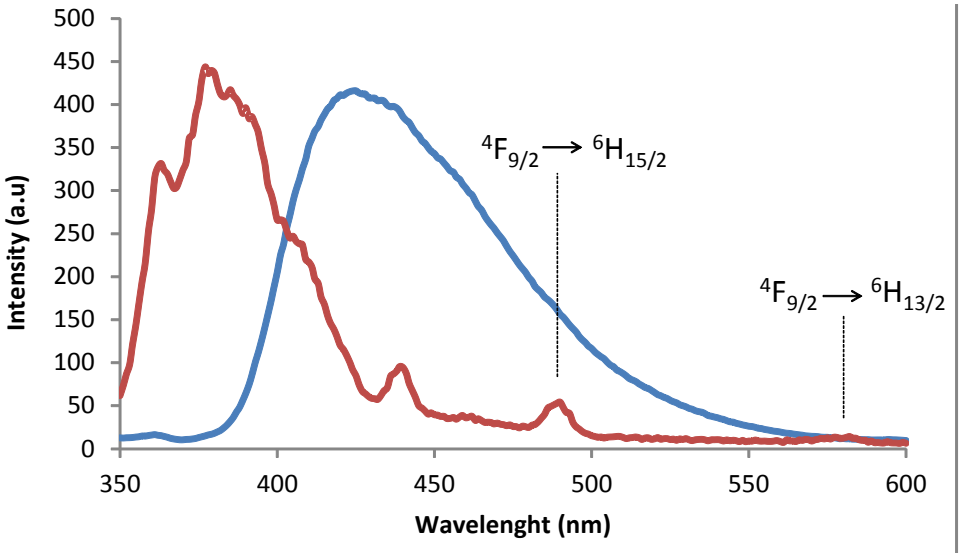

Figure S1. Solid-state emission spectrum of **1** at room temperature.

2. Magnetic properties

Experimental Section:

Alternating current magnetic measurements wereperformed on aPPMS (Physical Property Measurement System) - Quantum Design Model 6000 magnetometer by using an oscillating ac field of 3.5 G and ac frequencies ranging from 60 to 10 000 Hz.

Magnetic properties:

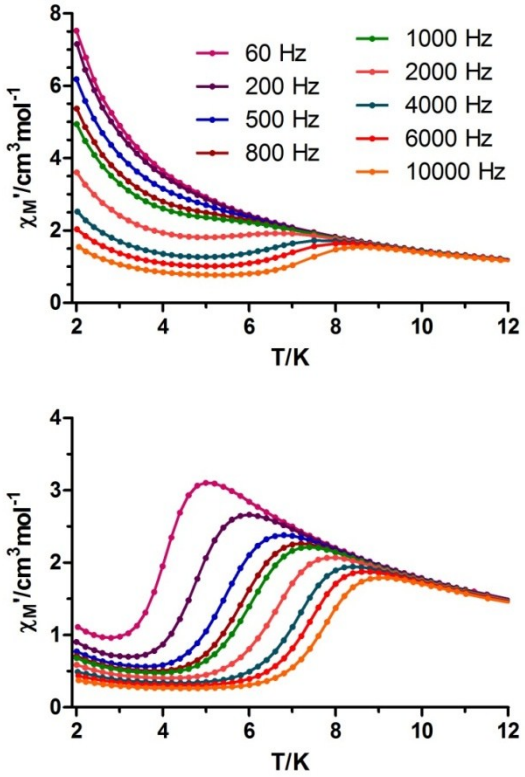

Figure S2. Temperature dependence of out-of-phase χ'_M component of the ac susceptibility for complex **1** measured under zero (top) and 1000 Oe (bottom) applied dc field.

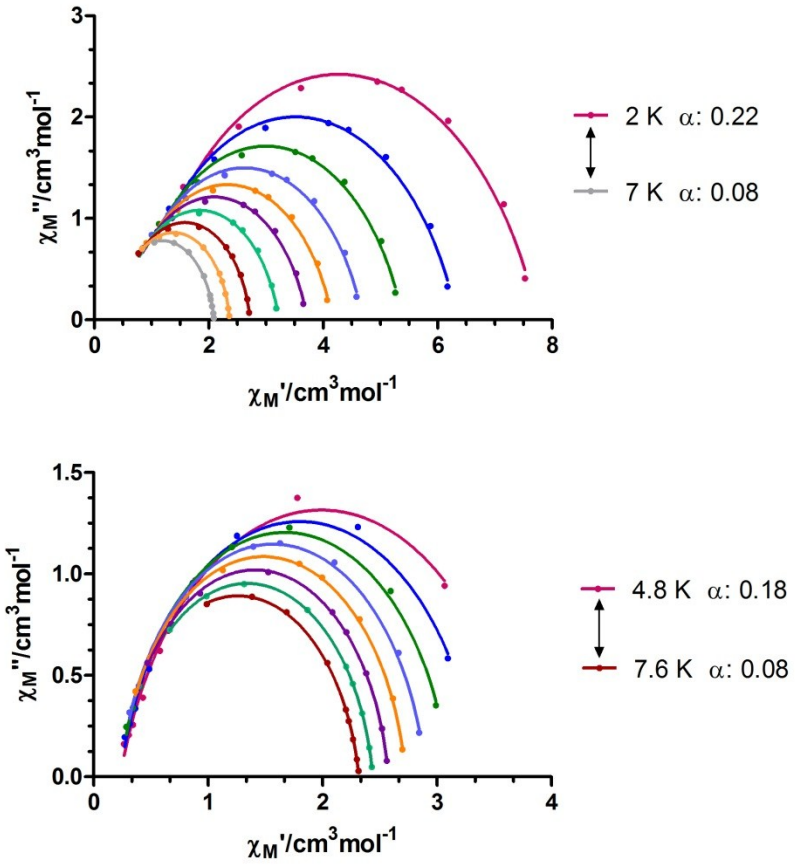

Figure S3. Cole-Cole plots for complex **1** measured under zero (top) and 1000 Oe (bottom) applied dc field.Solid lines represent the best fits to the generalized Debye model.

3. Biological properties

Material and Methods

In vitro cytotoxicity

The human colon tumor cell lines HT-29, DLD-1 and Caco-2 were provided by the European Collection of Authenticated Cell Cultures (ECACC, Salisbury, UK) through Sigma Aldrich Europe (Munchen, Germany). HT-29 cell line is BRAF-mutant, DLD-1 has the K-ras gene mutation, while Caco-2 is bearing mutations in APC, p53, and SMAD4, but not in K-ras or BRAF. The cell culture media used were: McCoy's 5 for HT-29, RPMI-1640 for DLD-1 and MEM with non-essential aminoacids for Caco-2, all supplemented with 10% fetal calf serum (media and supplements provided by Sigma Aldrich); the cells were growth as monolayer, subcultured before confluence. For the experiments they were seeded at a concentration of $1.5x10^5$ cells/ mL onto culture plates ($3x10^4$ cells in 200 µL for 96-well plates, $3x10^5$ cells in 2mL for 6-well culture plates); all plastic disposables were from Nunc, through Thermo Scientific, Waltham, USA.

MOF and the ligand were dissolved in RNAse free ultrapure water (from Sigma Aldrich), by stirring, gentle heat up to 50-60 Celsius degrees, and filtration through 0,22 µm syringe filters (Millex, from Millipore, USA) to obtain 20 mM sterile stock solutions. Serial dilutions were prepared using sterile phosphate buffered saline solution (PBS, from Sigma Aldrich); the working solutions were mixed with cell culture media to obtain a final concentration on cells in the range of 0.5-1000 µM.

To assess the cytotoxicity, the cells were treated for 24 hours, and than MTS viability assays were performed on the 96-well microplates (reagents from Promega Corporation, Madison, WI, USA). The wells were treated with 10 µL of MTS-PMS mix according to the manufacturer's indications, and after 4 hours of incubation, colorimetric measurements were performed with the Synergy2 microplate reader (from BioTek Company, Winooski, VT, USA) at 570nm. Untreated cells were used as references, and cell culture media for blank. Measurements were made in triplicate.

The half inhibitory concentrations (IC50) were calculated by the Graph Pad Prism 5 biostatistics (from GraphPad Software, La Jolla, USA), using the dose-response sigmoidal curves, $p<0.05$.

The cells capacity to proliferate was estimated using the Alamar blue staining (reagent from Molecular Probes Invitrogen, Eugene, USA) which indicates the reducing power of viable cells. The reagent was added to cells 24 hours after the treatment, the plates were incubated at 37 °C for 2 hours, and the fluorescence was measured with the Synergy 2.0 microplate reader at an excitation wavelength of 570 nm and emission at 620 nm. All tests were performed in triplicates.

For cells growth comparison between treated cell populations subjected to magnetic field and those with treatment only, $3x10^5$ cells in 2mL media were mixed in a proportion of 20:1 with MOF solutions having concentrations between 1-20 mM, immediately subjected to magnetic field for 20 minutes, than seeded onto culture plates for 24 hours, when MTS assay/Alamar Blue staining was performed, and the series of magnetized and un-magnetized were compared. As reference we used untreated cells.

Cell cultures exposure to magnetic field

The magnetic field was generated using pulse and arbitrary waveform generators Tabor Electronics Model WW5061 (Tel Hanan, Israel). The broadband amplifier was custom made, having a frequency range of 100 KHz-10 MHz, output power 1-200 W, a tuned circuit consisting of an inductor and a capacitor, connected together. The 11 ml conical bottom polycarbonate centrifuge tubes (from Nunc, Thermo Fisher Scientific) containing 2mL of cell suspension at a concentration of $1.5x10^5$ cells/ mL were placed in the circuit which can act as an electrical resonator, an electrical analogue of a tuning fork, storing energy oscillating at the circuit's resonant frequency. The time of exposure was 20 minutes, at an intensity of 0.1 Tesla of the magnetic field.

The reducing power of metabolically active tumor cells, quantified using the Alamar Blue staining, is an indicator of their capacity to proliferate and show a magnetic field dependence (Table S1).

The test was successfully applied in previous studies concerning lanthanides biologic activity. [1] In K-ras mutant DLD-1 cells and in Braf mutant HT-29 cells the MOF treatment alone can not diminish the proliferating potential of the tumor cells, whereas the MOF-treated and magnetized cells reducing capacity decreased significantly in compare with those non-irradiated (the differences between elevations are extremely significant). In Caco-2 population which is not bearing the above mentioned mutations, the proliferating capacity of the cells subjected to [DyNa(ampy)4] diminished, the effect was similar with magnetic irradiation as well (Table S1).

Early apoptotic processes

Apoptosis of treated DLD-1 and HT-29 cells was measured using Alexa Fluor 480-labeled AnnexinV marker, concomitant with the propidium iodide stain which indicates the death cells (reagents from Life Technologies, through Thermo Fisher Scientific, Waltham, USA). The cells were treated for 8 hours with MOF, at a concentration of $1x10^6$ cells/ mL, cells were harvested from the microplates, washed in cold PBS, resuspended in staining buffer. Samples were divided in two aliquots, stained with Alexa Fluor Annexin V, or with PI, respectively. After 15

[1] Y. Zhang, G. K. Das, V. Vijayaragavan, Q. C. Xu, P. Padmanabhan, K. K. Bhakoo, S. T. Selvan, T. T. Tan, *Nanoscale* **2014**, *6*, 12609.

minutes incubation, the cells were washed in cold PBS, resuspended in 100 µl buffer and the fluorescence was measured at 530-575 nm using 488 nm excitation, in triplicate.

Multidrug resistance

The inhibitory effect of MOF on MDR1 and MRP1 multidrug resistance proteins expresion was evaluated using a fluorescence-based kit (Ab112142 MDR assay kit from Abcam, Cambridge, UK). 24 hours after the cells treatment and magnetization the fluorescent sensor dye solved in DMSO was added to cell cultures in 96-well plates in 1:1 volume ratio, and after one hour of incubation fluorimetric measurements were performed with the Synergy 2 platform after 1 hour of incubation, at 485/20 emission with 620/40 absorption wavelength (nm).

However, not only an interesting cytotoxic behaviour is needed when designing new metallodrugs, but in the conventional cancer therapy the multidrug resistance is a serious limitation. Therefore, new drugs are needed to counterbalance this phenomenon. Thus, some studies on multidrug-resistance were carried out using $[DyNa(ampy)_4]$. The multidrug-resistance 1 (MDR-1) P-glycoprotein is a transmembrane transporter system, which actively pumps cytotoxic drugs out of the cell. [2] The colorectal carcinoma cell line DLD-1 overexpress MDR-1, while in HT-29 and Caco-2 its expression is limited. MRP1 expression could be barely detected only in DLD-1 cells. [3,4]

The expression of drug efflux pump MDR-1 was not suppressed by MOF in the aggressive DLD-1 population having basal multidrug resistance gene overexpression, but when the cells were treated and exposed to magnetic field a significant decrease was observed (Table S2). The magnetization provided a real benefit in counteracting the multidrug resistance. In HT-29 and Caco-2 cells having a lower basal expression of MDR1, this drug pump was inhibited by MOF treatment, and the outcome of treatment and simultaneous magnetization does not differ significantly.

The IC_{50} values corresponding to the treated and magnetized tumor cell populations (Table S1) highlight the differences of cytotoxicity. As can be seen in the Table S3 below in all cases, the IC50 values notably decreased, which denotes that the toxicity of compounds is higher when magnetization was applied.

---

2 U. Schumacher, N. Nehmann, E. Adam, D. Mukthar, I. N. Slotki, H. P. Horny, M. J. Flens, B. Schlegelberger, D. Steinemann, Acta Histochem. 2012, 114, 594.
3 L. Mayor-López, E. Tristante, M. Carballo-Santana, E. Carrasco-García, S. Grasso, P. García-Morales, M. Saceda, J. Luján, J. García-Solano, F. Carballo, C. de Torre, I. Martínez-Lacaci. Transl Oncol. 2014, 7, 590.
4 M. Yasunaga, Y. Matsumura, Sci Rep. 2014, 4, 4852.

Table S1. IC_{50} values in the absence and presence of magnetic field[a] for ligand and dysprosium complex against HT-29, DLD-1 and Caco-2.

Compound	$[DyNa(ampy)_4]_n$			$[DyNa(ampy)_4]_n$ and magnetic field			Ligand		
Cell line	IC_{50} (μM)	Log IC_{50}	SD LogIC_{50}	IC_{50} (μM)	Log IC_{50}	SD LogIC_{50}	IC_{50} (μM)	Log IC_{50}	SD LogIC_{50}
HT-29	87.1	1.940	0.201	74.97	1.875	0.041	339.8	2.531	0.192
DLD-1	174.9	2.243	0.125	142.7	2.154	0.086	426.3	2.630	0.206
Caco-2	248.8	2.396	0.117	181.2	2.258	0.056	>1000	-	-

[a] The intensity of the magnetic field was chosen according to the golden standard limits established by Atkinson in 2007 (Atkinson IC, Renteria L, Burd H, Pliskin NH, Thulborn KR. J Magn Reson Imaging. 2007; 26(5):1222-1227).

Table. S2. The capacity of MOF to reduce the living cells reducing potential, quantified by linear regression in the 95% confidence interval. The statistical significance of the deviation from 0 was quantified using the hill slope, the measure of goodness-of-fit of the linear regression (r^2), the relationship between the relative increases in sum-of-squares (F ratio), p being a quantification of the probability.

Tumor cell population	Type of treatment	Statistical parameters					Comparison between the MOF-treated cells subjected to magnetic field versus the unexposed ones
		Hillslope	r^2	F ratio	p	Deviation from 0	
DLD-1	Treated cells	-120.2 ± 57.76	0.2130	4.329	0.0539	Not Significant	The differences between the elevations are very significant, p=0.001189, F=12.5876
	Treated and exposed to magnetic field	-231.8 ± 39.71	0.6805	34.08	< 0.0001	Significant	
HT-29	Treated cells	-306.3 ± 158.9	0.1885	3.716	0.0718	Not Significant	The gradient of elevations differ significantly, p=0.003707, F=9.7569
	Treated and exposed to magnetic field	-291.4 ± 115.1	0.2862	6.415	0.0222	Significant	
Caco-2	Treated cells	-226.7 ± 98.38	0.2899	5.308	0.0384	Significant	The difference between the slopes and elevations are not significant, p=0.8442, F=0.03935
	Treated and exposed to magnetic field	-174.4 ± 72.27	0.3094	5.825	0.0313	Significant	

Table S3. The modulation of multidrug resistance proteins by in vitro application of MOF and the exposure of treated colon cell lines to magnetic field.

Tumor cell population	Type of treatment	Statistical parameters					Comparison between the MOF-treated cells subjected to magnetic field versus the unexposed ones
		Hillslope	r^2	F ratio	p	Deviation from 0	
DLD-1	Treated cells	-7.124 ± 3.571	0.2847	3.981	0.0740	Not significant	The differences between the rates of decrease in magnetized vs. unexposed samples are extremely significant, F= 29.7897 and p<0.0001
	Treated and exposed to magnetic field	-10.28 ± 2.025	0.7204	25.76	0.0005	Significant	
HT-29	Treated cells	-9.854 ± 1.899	0.7291	26.91	0.0004	Significant	The differences between elevations are not significant, F= 0.0066 and p=0.936
	Treated and exposed to magnetic field	-9.575 ± 2.230	0.6484	18.44	0.0016	Significant	
Caco-2	Treated cells	-14.28 ± 3.179	0.7162	20.19	0.0020	Significant	The differences between elevations are not significant, F= 0.7097 and p=0.4112
	Treated and exposed to magnetic field	-13.92 ± 3.695	0.6395	14.19	0.0055	Significant	

4. Synthesis of 1

The preparation of $[DyNa(ampy)_4]_n$ is very simple and is achieved via the soft hydrothermal reaction of the dysprosium nitrate (1 mmol, 22.4 mg), NaOH (0.1 mmol) and 5-aminopyridine-2-carboxylic acid (4 mmol, 6.9 mg) in dimethylformamide (10 ml) at 95 ºC for 24 h to give prismatic crystals of compound **1**. Anal. calcd. for $C_{24}H_{20}DyN_8NaO_8$: C, 39.27; N, 15.27; H, 2.75. Found: C, 39.11; N, 15.31; H, 2.71. FT-IR (ν_{max}/cm^{-1}): 3416(m), 3340(m), 3232(m), 1718(w), 1610(s), 1574(s), 1479(m), 1422(w), 1364(s), 1285(m), 1176(m), 1087(m), 1017(w), 800(w), 701(w) cm^{-1}.

Elemental analyses were carried out at the "Centro de Instrumentación Científica" (University of Granada) on a Fisons–Carlo Erba analyzer model EA 1108. FT-IR spectra on powdered samples were recorded with a ThermoNicolet IR200FTIR using KBr pellets.

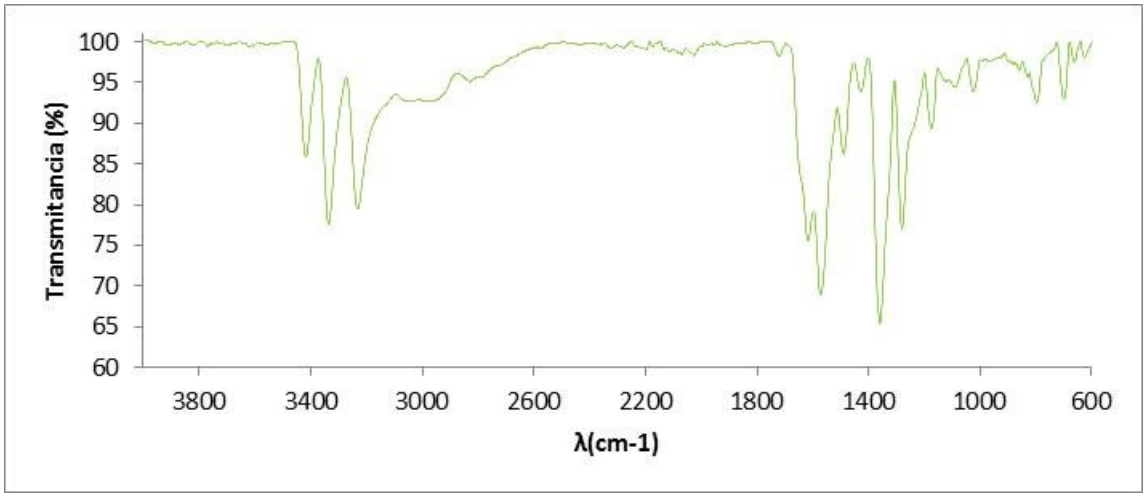

Figure S4. Infrared spectrum of **1** in KBr.

5. Crystal Data

Prismatic colourless crystals of compound **1** suitable for X-ray experiments were obtained. A crystal was resin epoxy coated and mounted on a on a Bruker D8 Venture with Photon detector equipped with graphite monochromated MoKα radiation (λ=0.71073 Å), operating at 50kV and a temperature of 100 K. The cell parameters were determined and refined by least-squares fit of all reflections collected. The first 100 frames were recollected at the end of the data collection to monitor crystal decay, and no appreciable decay was observed. In four cases, an empirical absorption correction was applied. The data reduction was performed with the APEX2[5] software

5.- A. Bruker, Inc. APEX2 (Version 1.08), SAINT (Version 7.03), SADABS (Version 2.11), SHELXTL

and corrected for absorption using SADABS.[6] Crystal structures were solved by direct methods using the SIR97 program[7] and refined by full-matrix least-squares on F^2 including all reflections using anisotropic displacement parameters by means of the WINGX crystallographic package.[8] In all cases, the hydrogen atoms were included with at their calculated positions determined by molecular geometry and refined riding on the corresponding bonded atom. Final $R(F)$, $wR(F^2)$ and goodness of fit agreement factors, details on the data collection and analysis can be found in Table S4. CCDC 1444210 contain the supplementary crystallographic data for this paper. These data can be obtained free of charge from The Cambridge Crystallographic Data Centre via Crystallographic Data Centre via www.ccdc.cam.ac.uk/data_request/cif.

Table S4. Crystallographic Data for compound **1**

Compound	**1**
chemical formula	$C_{24}H_{20}N_8O_8DyNa$
M/gmol^{-1}	733.97
CCDC	1444210
T (K)	100
λ/Å	0.71073
cryst syst	tetragonal
space group	$I4_1/a$
a/ Å	18.0441(8)
c/ Å	8.3135(7)
V/ Å^3	2706.8(3)
Z	4
ρ(g cm-3)	1.801
μ(mm-1)	2.840
Unique reflections	24638
R(*int*)	0.082
GOF on F^2	1.231
R1 [I > 2σ(*I*)] [a]	0.046
wR2 [I > 2σ(*I*)] [a]	0.121
[a] $R(F) = \sum\|\|F_o\| - \|F_c\|\|/\sum\|F_o\|$; $wR(F^2) = [\sum w(F_o^2 - F_c^2)^2/\sum wF^4]^{1/2}$	

(Version 6.12), Bruker Advanced X-ray Solutions, Madison, DOI (2004).

6.- G. Sheldrick, Sadabs, University of Göttingen, Germany Program for Empirical Absorption Correction of Area Detector Data 1996.

7.- A. Altomare, M.C. Burla, M. Camalli, G.L. Cascarano, C. Giacovazzo, A. Guagliardi, A.G.G. Moliterni, G. Polidori, R. Spagna, SIR97: a new tool for crystal structure determination and refinement, J. Appl. Crystallog., 1999, 32, 115.

8.- (a) G.M. Sheldrick, Program for Crystal Structure Refinement, University of Göttingen, Göttingen, Germany, 2014. (b) L.J. Farrugia, WinGX suite for small-molecule single-crystal crystallography, J. Appl. Crystallog., 1999, 32, 837-838.

Table S5. Bond distances (Å) and angles (º) for compound **1**

Bond Distances	**Bond Angles**
Dy1 O1 2.311(5)	O1 Dy1 O1 132.84(15)
Dy1 O1 2.311(5)	O1 Dy1 O1 68.9(2)
Dy1 O1 2.311(5)	O1 Dy1 N1 82.42(16)
Dy1 O1 2.311(5)	O1 Dy1 N1 134.54(18)
Dy1 N1 2.555(5)	O1 Dy1 N1 80.95(16)
Dy1 N1 2.555(5)	O1 Dy1 N1 65.65(18)
Dy1 N1 2.555(5)	N1 Dy1 N1 91.76(5)
Dy1 N1 2.555(5)	N1 Dy1 N1 159.8(3)
Na1 O1 2.603(5)	O1 Na1 O1 138.40(13)
Na1 O1 2.603(5)	O1 Na1 O1 60.29(19)
Na1 O1 2.603(5)	
Na1 O1 2.603(5)	

6. Continuous Shape Measurements

Table S6.- Continuous Shape Measurements for the LnO_8 coordination environment. Low values indicate high proximity to the analyzed ideal geometry.

OP-8	1 D_{8h}	Octagon
HPY-8	2 C_{7v}	Heptagonal pyramid
HBPY-8	3 D_{6h}	Hexagonal bipyramid
CU-8	4 O_h	Cube
SAPR-8	5 D_{4d}	Square antiprism
TDD-8	6 D_{2d}	Triangular dodecahedron
JGBF-8	7 D_{2d}	Johnson gyrobifastigium J26
JETBPY-8	8 D_{3h}	Johnson elongated triangular bipyramid J14
JBTPR-8	9 C_{2v}	Biaugmented trigonal prism J50
BTPR-8	10 C_{2v}	Biaugmented trigonal prism
JSD-8	11 D_{2d}	Snub diphenoid J84
TT-8	12 T_d	Triakis tetrahedron
ETBPY-8	13 D_{3h}	Elongated trigonal bipyramid

	OP-8	**HPY-8**	**HBPY-8**	**CU-8**	**SAPR-8**	**TDD-8**	**JGBF-8**
Comp 1	34.972	25.374	14.024	12.064	4.610	2.069	12.535

	JETBPY-8	**JBTPR-8**	**BTPR-8**	**JSD-8**	**TT-8**	**ETBPY-8**
Comp 1	29.749	5.167	3.913	5.021	12.886	24.515